PROCEEDINGS OF SCIENCE

Pion–nucleon scattering: from chiral perturbation theory to Roy–Steiner equations

Bastian Kubis and Jacobo Ruiz de Elvira[*†]
Helmholtz-Institut für Strahlen- und Kernphysik (Theorie) and
Bethe Center for Theoretical Physics, Universität Bonn, D–53115 Bonn, Germany
E-mail: kubis@hiskp.uni-bonn.de, elvira@hiskp.uni-bonn.de

Martin Hoferichter
Institute for Nuclear Theory, University of Washington, Seattle, WA 98195-1550, USA
E-mail: mhofer@uw.edu

Ulf-G. Meißner
Helmholtz-Institut für Strahlen- und Kernphysik (Theorie) and
Bethe Center for Theoretical Physics, Universität Bonn, D–53115 Bonn
Institut für Kernphysik, Institute for Advanced Simulation, Jülich Center for Hadron Physics,
JARA-HPC, and JARA-FAME, Forschungszentrum Jülich, D–52425 Jülich, Germany
E-mail: meissner@hiskp.uni-bonn.de

Ever since Weinberg's seminal predictions of the pion–nucleon scattering amplitudes at threshold, this process has been of central interest for the study of chiral dynamics involving nucleons. Quantities like the scattering lengths or the pion–nucleon σ-term are fundamental characteristics of the explicit breaking of chiral symmetry by means of the light quark masses. On the other hand, pion–nucleon dynamics also strongly affects the long-range part of nucleon–nucleon potentials, and hence has a far-reaching impact on nuclear physics. We briefly review approaches to analyze pion–nucleon scattering in the framework of baryon chiral perturbation theory. We then discuss how the fruitful combination of dispersion-theoretical methods, in particular in the form of Roy–Steiner equations, with chiral dynamics allows for a precise determination of pion–nucleon scattering amplitudes at low energies. Special attention will be paid to the extraction of the pion–nucleon σ-term and the low-energy constants of chiral perturbation theory.

The 8th International Workshop on Chiral Dynamics, CD2015 ***
29 June 2015–03 July 2015
Pisa, Italy

[*]Speakers.

[†]This writeup is the combined proceedings contribution summarizing the two talks "Pion–nucleon scattering at low energies" by Bastian Kubis and "Precise dispersive determination of πN scattering and the σ-term" by Jacobo Ruiz de Elvira.

PoS(CD15)021

Figure 1: (a) Leading-order diagrams for πN scattering in chiral perturbation theory. Nucleons are denoted by full, pions by dashed lines. (b) Next-to-leading-order diagrams, depending on low-energy constants c_{1-4}. These diagrams capture the leading effect of $\Delta(1232)$ resonance exchange. Crossed Born terms and Δ exchange graphs are not shown explicitly.

1. Introduction

Pion–nucleon (πN) scattering is one of the simplest processes to study chiral dynamics involving nucleons. At leading order (LO) in the chiral expansion, i.e., in the expansion in pion masses and momenta, the scattering amplitude is given by the Feynman diagrams shown in Fig. 1, resulting in the well-known low-energy theorems (LETs) for the S-wave scattering lengths, the amplitudes evaluated at threshold [1, 2]:

$$a_{0+}^- = \frac{M_\pi m_N}{8\pi(m_N+M_\pi)F_\pi^2} + \mathcal{O}\big(M_\pi^3\big), \qquad a_{0+}^+ = \mathcal{O}\big(M_\pi^2\big). \tag{1.1}$$

The isospin-odd scattering length is hence predicted solely in terms of the pion (M_π) and nucleon (m_N) masses as well as the pion decay constant F_π, while the isospin-even one is suppressed. The strength of the Born term amplitudes (that do not contribute at threshold to leading order) is given in terms of the pion–nucleon coupling constant g, which is related to the axial coupling g_A by the Goldberger–Treiman relation, $g = g_A m_N/F_\pi$, up to higher orders.

Already at next-to-leading order (NLO; $\mathcal{O}(p^2)$ in the chiral counting), the πN scattering amplitude depends on a list of low-energy constants (LECs), conventionally denoted by c_{1-4}, which are less readily determined from phenomenology. These NLO contributions tend to be large: three of the couplings (c_{2-4}) incorporate the leading low-energy effects of the $\Delta(1232)$, the lowest-lying resonant excitation of the nucleon; see also Fig. 1. As the mass gap is small, $m_\Delta - m_N \sim 2M_\pi$, and as the Δ couples strongly to the πN system, the numerical values of the NLO LECs are somewhat larger than expected from naive dimensional analysis. To pin down these LECs accurately and consistently is an important task also in view of many nuclear physics applications: as shown in Fig. 2, πN amplitudes constitute an important contribution to the two-pion exchange in nucleon–nucleon scattering potentials, and determine the leading long-range three-nucleon force.

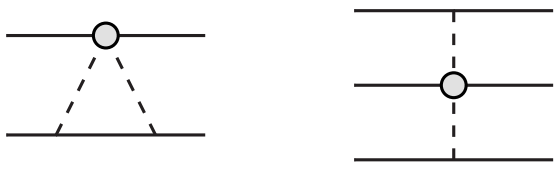

Figure 2: Contributions of pion–nucleon amplitudes to nucleon–nucleon scattering (left) and the three-nucleon force (right). The gray blob denotes πN-scattering-type subdiagrams.

A further strong incentive to study pion–nucleon scattering derives from its relation to the pion–nucleon σ-term $\sigma_{\pi N}$, defined via the scalar form factor of the nucleon

$$\sigma(t) = \frac{1}{2m_N}\langle N(p')|\hat{m}(\bar{u}u + \bar{d}d)|N(p)\rangle, \qquad \hat{m} = \frac{m_u + m_d}{2}, \qquad \sigma_{\pi N} \equiv \sigma(0), \tag{1.2}$$

where $t = (p'-p)^2$. Through the Feynman–Hellmann theorem [3, 4], $\sigma_{\pi N}$ determines the light-quark content of the nucleon mass,

$$\sigma_{\pi N} = \hat{m}\frac{\partial m_N}{\partial \hat{m}} = -4c_1 M_\pi^2 + \mathcal{O}(M_\pi^3), \tag{1.3}$$

where we have already indicated the leading term in the chiral expansion of this quantity: it is given in terms of the LEC c_1, which in turn should be fixed from πN scattering. This is the leading approximation to the Cheng–Dashen LET [5], which we will discuss in more detail below. The σ-term has garnered strong interest beyond the hadron physics community in recent years, due to its relation to the scalar couplings of the nucleon that are prerequisite for a consistent interpretation of direct-detection dark matter searches [6, 7, 8].

2. Chiral perturbation theory and πN scattering

It is well known that the extension of chiral perturbation theory (ChPT) [9, 10, 11] to include nucleons as massive matter fields is not without problems, in particular when it comes to including loop corrections. In contrast to the Goldstone boson theory, in which all mass scales are small, and naive dimensional counting works as long as a mass-independent regularization scheme such as dimensional regularization is used to calculate loop diagrams, the nucleon mass constitutes a new mass scale of the order of the chiral symmetry breaking scale, $m_N \approx \Lambda_\chi = 4\pi F_\pi \sim 1\,\text{GeV}$. Loop integrals pick up contributions from momenta of the order of the nucleon mass, with the result that loops that should be suppressed in the chiral expansion in fact renormalize lower-order coupling constants [12]. Various schemes have been used to overcome this problem.

- The heavy-baryon expansion [13, 14] regards the nucleon as heavy, non-relativistic fields; nucleon momenta are decomposed into a large component proportional to the nucleon's velocity, plus small, residual momenta of the order of the pion mass. Similarly to heavy-quark effective field theory, the non-relativistic expansion eliminates the mass from the nucleon propagator, which re-enters parametrically in inverse powers as $1/m_N$ corrections, which can be constructed systematically on the Lagrangian level [14]. As a result, a two-fold expansion is performed, with a unified power counting scheme $p/\Lambda_\chi \sim p/m_N$.[1]

- The infrared regularization (IR) scheme [15, 16], in contrast, is a manifestly covariant prescription, in which loop integrals are divided into an infrared singular and a regular part. The infrared singular part contains all non-analytic loop effects and obeys naive power counting rules, while the regular part can be expanded in a polynomial in p^2 and M_π^2 and can be consistently reabsorbed into a redefinition of the counterterms.

[1] An alternative counting scheme is typically used in NN applications, where the generic breakdown scale Λ_b is assumed to be smaller, and recoil corrections are deferred to higher orders by counting $p/m_N \sim (p/\Lambda_\text{b})^2$.

- In the IR prescription, regular parts of loop integrals are subtracted completely, which has the disadvantage of inducing unphysical cuts outside the low-energy region [16]. This can be avoided in the extended on-mass-shell (EOMS) scheme [17, 18], where only the explicitly power-counting-violating terms, expanded as a polynomial to the necessary order, are omitted, thus preserving the correct analytic structure of the relativistic loop graphs.

Ultimately, these regularization schemes of baryon ChPT, which have all been applied to analyze πN scattering, should be equivalent (up to incomplete higher orders) when applied in "safe" kinematical regimes, away from branch cut singularities. In contrast, it has been shown that a naive heavy-baryon representation of triangle loop graphs does not converge in the complete low-energy region [16]; e.g., the spectral functions of nucleon electromagnetic form factors show the wrong threshold behavior due to the heavy-baryon approximation of anomalous thresholds [19], while these are correctly reproduced in covariant schemes such as the IR one [20].

Apart from the use of various loop regularization schemes, different ChPT-based studies of πN scattering also differ in the treatment of the $\Delta(1232)$ resonance. As we explained above, Δ contributions enhance some of the LECs significantly; e.g. the contributions to c_{2-4} as determined from the resonance saturation hypothesis can be as large as [21]

$$c_2^\Delta = -c_3^\Delta = 2c_4^\Delta \approx 3.8\,\mathrm{GeV}^{-1}, \tag{2.1}$$

which slows down the convergence of the chiral expansion significantly. It has therefore been proposed to include the Δ degrees of freedom dynamically in baryon ChPT [22], which is also plausible with regards to the large-N_c limit, in which the nucleon and the Δ become mass-degenerate. Unified counting schemes that have been suggested for this combined effective theory include the ε expansion [23], in which p, M_π, and $m_\Delta - m_N$ are all counted as $\mathcal{O}(\varepsilon)$, and an alternative δ expansion [24], in which $p, M_\pi \sim \mathcal{O}(\delta)$, but $m_\Delta - m_N \sim \mathcal{O}(\delta^{1/2})$ at low energies or near threshold, such that loops including Δ propagators are effectively shifted to higher orders.

A significant number of studies over the last few years has pursued the strategy to fix πN LECs by fitting to existing phase-shift analyses: the dispersion-theory-based Karlsruhe–Helsinki analysis [25, 26], the GWU/SAID solution that is continuously updated with the latest data [27, 28], in some cases also the analysis performed by the Zürich group [29]. As ChPT obeys unitarity in a perturbative sense only, amplitudes are usually unitarized by dropping the imaginary part and reconstructing the phase shift from the real part only according to the prescription

$$\delta(s) = \arctan\left(\frac{|\mathbf{q}|}{8\pi\sqrt{s}}\mathrm{Re}\,t(s)\right) \approx \frac{|\mathbf{q}|}{8\pi\sqrt{s}}\mathrm{Re}\,t(s), \tag{2.2}$$

where $t(s)$ is a generic partial wave, and $\mathbf{q}$ the center-of-mass 3-momentum. The number of LECs to be fitted at the different chiral orders is four c_i at $\mathcal{O}(p^2)$, four (linear combinations of) $\bar{d}_i$ at $\mathcal{O}(p^3)$ (plus one additional constant, $\bar{d}_{18}$, that parametrizes the Goldberger–Treiman discrepancy in cases where the pion–nucleon coupling was not assumed to be fixed), and five (combinations of) $\bar{e}_i$ at $\mathcal{O}(p^4)$, which corresponds to complete one-loop order. Studies of this kind, performed over the last five years only, include IR to $\mathcal{O}(p^3)$ [30], EOMS to $\mathcal{O}(p^3)$ and $\mathcal{O}(\delta^3)$ [31], EOMS to $\mathcal{O}(p^4)$ and $\mathcal{O}(\delta^3)$ [32] (the amplitudes including the Δ calculated in this study may violate certain positivity constraints inside the Mandelstam triangle [33]), heavy-baryon ChPT to $\mathcal{O}(p^4)$ with

NN counting scheme [34], an analysis of fitting the amplitudes of [34] to actual observables instead of phase shifts [35], and an $\mathcal{O}(p^3)$ amplitude with N/D unitarization and CDD poles for the Δ as well as the $N(1440)$ [36]. Fit ranges typically extend up to about $\sqrt{s} \approx 1.13\,\text{GeV}$ without, and 1.20 GeV with the Δ included explicitly. In most cases, the σ-terms extracted correspond to the phase-shift analyses used as input: values like $\sigma_{\pi N} \sim 45\,\text{MeV}$ are derived from fitting to the Karlsruhe–Helsinki analysis, while $\sigma_{\pi N} \sim 60\,\text{MeV}$ is typically obtained from the GWU/SAID solution. Reliable estimates of the uncertainties associated with these values are difficult, in particular in view of the extrapolation of the chiral amplitudes from the scattering into the physical region.

We will therefore follow a different strategy in the following, and instead of using ChPT directly, analyze πN scattering using dispersion theory, in the particular form of Roy–Steiner equations. We will come back to the issue of matching to ChPT in Sect. 8 only.

The following presentation relies heavily on our original article [37].

3. Roy–Steiner equations for πN scattering

In recent years, it has become apparent that the predictive power of chiral symmetry can be vastly increased by combining ChPT with dispersive techniques, which exploit analyticity to arrive at a representation that relates the amplitude at an arbitrary point in the complex plane to an integral over its imaginary part. While the latter can be constrained by the respective unitarity relation, convergence of the dispersive integral often requires a certain number of a priori undetermined subtraction constants that, in turn, can frequently be pinned down by matching to ChPT. Once the subtraction constants are fixed, a dispersive representation provides the ideal framework to reliably perform an analytic continuation into the complex plane, which becomes of fundamental importance for broad resonances situated far away from the real axis.

In particular, for $\pi\pi$ scattering, the use of Roy equations [38] has led to a determination of the low-energy $\pi\pi$ scattering amplitude with unprecedented accuracy [39, 40]. They are obtained from a twice-subtracted fixed-t dispersion relation, where the t-dependent subtraction constants are determined by means of $s \leftrightarrow t$ crossing symmetry, and performing a partial-wave expansion. This leads to a coupled system of partial-wave dispersion relations (PWDRs) for the $\pi\pi$ partial waves $t_J^I(s)$ with isospin I and angular momentum J

$$t_J^I(s) = S_J^I(s) + \sum_{I'=0}^{2} \sum_{J'=0}^{\infty} \int_{4M_\pi^2}^{\infty} \mathrm{d}s' K_{JJ'}^{II'}(s,s') \,\mathrm{Im}\, t_{J'}^{I'}(s'), \tag{3.1}$$

where $K_{JJ'}^{II'}$ are known kinematical kernel functions and the scattering lengths—the only free parameters—appear in the subtraction terms $S_J^I(s)$. In addition, assuming elastic unitarity

$$\mathrm{Im}\, t_J^I(s) = \sigma(s) |t_J^I(s)|^2, \quad t_J^I(s) = \frac{e^{2i\delta_J^I(s)} - 1}{2i\sigma(s)}, \quad \sigma(s) = \sqrt{1 - \frac{4M_\pi^2}{s}}, \tag{3.2}$$

(3.1) translates into a coupled integral equation for the phase shifts δ_J^I themselves.

An important issue is the range of validity of the Roy equations. While the convergence of the fixed-t dispersion relations is guaranteed for all $t < 4M_\pi^2$ [41, 42, 43], the reduction to partial waves imposes further constraints on the domain of validity of the system. As a matter of fact, the

partial-wave expansion of the imaginary part in the dispersive integral converges only for scattering angles z' that lie within the large Lehmann ellipse [44]. Due to the finite domain of validity, the Roy equations cannot be used up to infinity. Above a certain energy, referred to as the matching point s_m, input from experiment for the imaginary parts of the partial waves is required, so that in practice the equations are solved between threshold and s_m. Furthermore, the partial-wave expansion will be truncated at a certain angular momentum J and higher partial waves treated on the same footing as the lower partial waves above s_m.

Unfortunately, in the case of πN scattering, a full system of PWDRs has to include dispersion relations for two distinct physical processes, $\pi N \to \pi N$ (s-channel) and $\pi\pi \to \bar{N}N$ (t-channel), and the use of $s \leftrightarrow t$ crossing symmetry will intertwine s- and t-channel equations, which hampers the use of fixed-t dispersion relations for this system.

Roy–Steiner (RS) equations are also a set of coupled PWDRs that, in contrast to $\pi\pi$ Roy equations, are derived from hyperbolic dispersion relations (HDRs) [45], which automatically relate the different channels in the πN system. In close analogy to similar analyses of the $\pi\pi$ [39], the πK [46], or the $\gamma\pi$ [47] system, solving the RS equations for πN, in particular once combined with the pionic-atom constraints on the scattering lengths [48, 49], can provide a remarkably precise representation of the πN amplitude at low energies.

The construction of a complete system of RS equations for πN scattering has been presented in detail in [50]; see also [51, 52, 53] for partial results. The starting point in the derivation is provided by HDRs for the invariant πN amplitudes, which, in combination with the pertinent partial-wave expansions as well as unitarity relations, are used to derive a closed system of PWDRs that fully respects analyticity, unitarity, and crossing symmetry. Subtractions are performed at the so-called subthreshold point $s = u$, $t = 0$, which proves convenient for the matching to ChPT and for the extrapolation to the Cheng–Dashen point [5], and thus for establishing the relation to $\sigma_{\pi N}$ by means of a low-energy theorem [5]. In fact, it has been pointed out previously that a reliable extrapolation to the subthreshold region requires additional input from the t-channel ($\pi\pi \to \bar{N}N$) partial waves [54, 55, 56], a requirement that is straightforward to comply with in the RS formalism, as HDRs by construction intertwine all physical regions. In the end, both the s- and t-channel equations will involve the subtraction constants and the πN coupling constant as free parameters, see [50]. In this way, the s-channel RS equations read [45]

$$\begin{aligned} f_{l+}^I(W) = N_{l+}^I(W) &+ \frac{1}{\pi}\int_{t_\pi}^{\infty} \mathrm{d}t' \sum_J \Big\{ G_{lJ}(W,t')\,\mathrm{Im}\, f_+^J(t') + H_{lJ}(W,t')\,\mathrm{Im}\, f_-^J(t') \Big\} \\ &+ \frac{1}{\pi}\int_{W_+}^{\infty} \mathrm{d}W' \sum_{l'=0}^{\infty} \Big\{ K_{ll'}^I(W,W')\,\mathrm{Im}\, f_{l'+}^I(W') + K_{ll'}^I(W,-W')\,\mathrm{Im}\, f_{(l'+1)-}^I(W') \Big\}, \end{aligned} \tag{3.3}$$

where due to G-parity only even/odd J contribute for isospin $I = +/-$, respectively. The kernels $K_{ll'}^I(W,W)$, $G_{lJ}(W,t)$, and $H_{lJ}(W,t)$ are known analytically, and $N_{l+}^I(W)$ denotes the partial-wave projections of the pole terms.

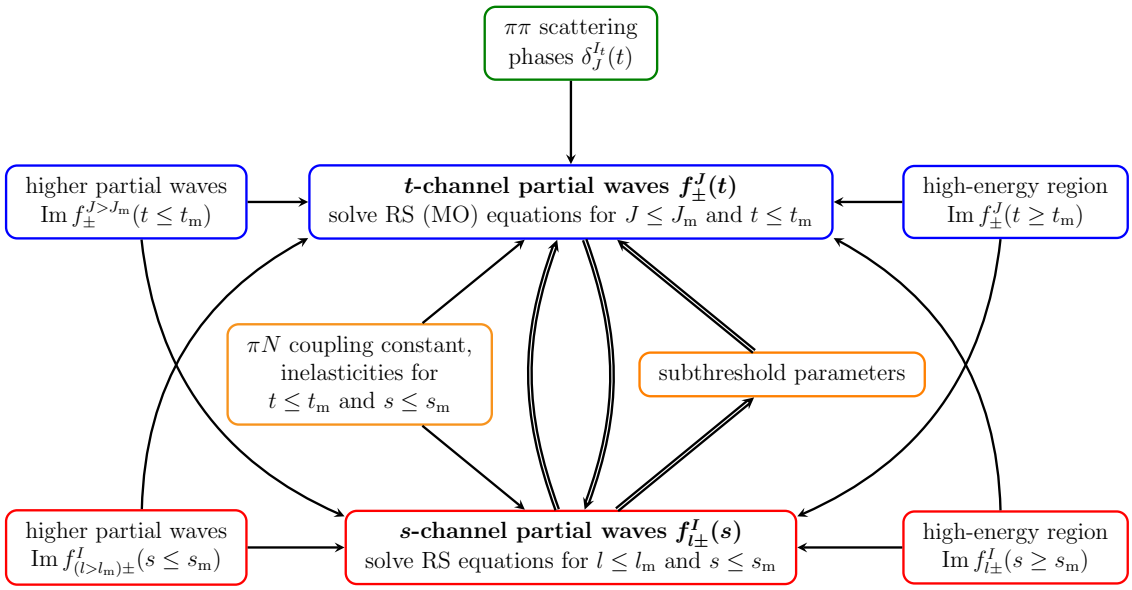

Figure 3: Solution strategy for RS equations in πN scattering. The s- and t-channel partial waves will be solved for up to angular momenta $l_\mathrm{m} = 1$ and $J_\mathrm{m} = 2$, respectively. Figure taken from [37].

For the t-channel partial-wave projection, the corresponding t-channel RS equations are [50]

$$f_+^J(t) = \tilde{N}_+^J(t) + \frac{1}{\pi}\int\limits_{t_\pi}^{\infty} \mathrm{d}t' \sum_{J'} \left\{ \tilde{K}^1_{JJ'}(t,t')\,\mathrm{Im}\, f_+^{J'}(t') + \tilde{K}^2_{JJ'}(t,t')\,\mathrm{Im}\, f_-^{J'}(t') \right\}$$
$$+ \frac{1}{\pi}\int\limits_{W_+}^{\infty} \mathrm{d}W' \sum_{\ell=0}^{\infty} \left\{ \tilde{G}_{J\ell}(t,W')\,\mathrm{Im}\, f^I_{\ell+}(W') + \tilde{G}_{J\ell}(t,-W')\,\mathrm{Im}\, f^I_{(\ell+1)-}(W') \right\}, \qquad (3.4)$$

and similarly for f_-^J except for the fact that these do not receive contributions from f_+^J. In addition, only even or odd J' couple to even or odd J (corresponding to t-channel isospin $I_t = 0$ or $I_t = 1$), respectively, and only higher t-channel partial waves contribute to lower ones.

Contrary to the s-channel, below the first inelastic threshold, the t-channel unitarity relations are linear in $f_\pm^J$

$$\mathrm{Im}\, f_\pm^J(t) = \sigma_t^\pi \left(t_J^{I_t}(t)\right)^* f_\pm^J(t), \qquad (3.5)$$

from which one can infer Watson's final-state interaction theorem [57], stating that (in the elastic region) the phase of $f_\pm^J$ is given by the phase $\delta_J^{I_t}$ of the respective $\pi\pi$ scattering partial wave $t_J^{I_t}$.

The strategy for the solution of the RS equations is outlined in Fig. 3: in the s-channel, the six S- and P-waves $f^I_{l\pm}$, with $I = \pm$ for the isospin index, orbital angular momentum l, and total angular momentum $j = |l \pm 1/2|$, are considered dynamically below the matching point s_m, whereas the imaginary parts of higher partial waves for all s, the imaginary parts of the S- and P-waves above s_m, and, potentially, inelasticities below s_m are required as input. In practice, we will choose the matching point at its optimal value $s_\mathrm{m} = (1.38\,\mathrm{GeV})^2$ as argued in [50]. In contrast to the six s-channel amplitudes, there are only three S- and P-waves in the t-channel, $f_\pm^J$, with total angular momentum J and the subscript referring to parallel/antiparallel antinucleon–nucleon helicities. The equations for the t-channel partial waves take the form of a Muskhelishvili–Omnès (MO)

problem [58, 59], whose solution requires—in addition to higher partial waves and the imaginary parts above the matching point t_m—input for the $\pi\pi$ phase shifts.

Once the t-channel problem is solved, the resulting t-channel partial waves are used as input for the s-channel problem, which then reduces to the form of conventional $\pi\pi$ Roy equations. Eventually, a full solution of the system can be obtained by iterating this procedure until all partial waves and parameters are determined self-consistently. In practice, virtually all interdependence proceeds via the subtractions constants, so that the need for an iterative procedure can be avoided if the corresponding terms are included explicitly in the s-channel fit.

4. Solutions of the t-channel and s-channel subproblems

Given that data in the t-channel reaction $\pi\pi \to \bar{N}N$ become available only above the two-nucleon threshold, the solution of the t-channel equations is subject to an additional complication that is related to the large pseudophysical region in this reaction. Thus, the amplitudes in the pseudophysical region $t_\pi \le t \le t_N$ required for the t-channel integrals need to be reconstructed from unitarity. While for every partial wave $\pi\pi$ intermediate states generate by far the dominant contribution, intermediate states besides $\pi\pi$ become relevant in the unitarity relation around 1 GeV, most notably in the S-wave, where $\bar{K}K$ intermediate states account for the occurrence of the $f_0(980)$ resonance, but also for all partial waves where inelasticities from the 4π channel start setting in before the two-nucleon threshold is reached. An explicit coupled-channel framework is only feasible if the corresponding S-matrix is known sufficiently accurately, a requirement that in the present application is only met for the $\pi\pi/\bar{K}K$ S-wave system. For this reason, we adopt a single-channel framework for P- and D-waves, estimating the impact of 4π inelasticities by appropriate variations of the input. Similarly, we include the $\bar{K}K$ channel explicitly in the S-wave, while accounting for effects from higher channels in the uncertainty estimate.

In the single-channel approximation, where only $\pi\pi$ intermediate states are considered in the unitarity relation, the MO solution for $f_\pm^J(t)$ is given in terms of the Omnès function [59]

$$\Omega_J(t) = \exp\left\{\frac{t}{\pi}\int\limits_{t_\pi}^{t_\mathrm{m}} \mathrm{d}t' \frac{\delta_J(t')}{t'(t'-t)}\right\}, \tag{4.1}$$

which is a function of the $\pi\pi$ phase shift $\delta_J(t)$ for angular momentum J (and isospin $0/1$ for even/odd J) only. Above t_m, further information about absorptive parts is required. However, in the practical application the uncertainties below t_m are much larger than the contribution from the imaginary part above, so that we will drop their contribution everywhere.

In the two-channel approximation the $\pi\pi \to \bar{N}N$ and $\bar{K}K \to \bar{N}N$ S-waves $f_+^0(t)$ and $h_+^0(t)$ fulfill the unitarity relation

$$\mathrm{Im}\,\mathbf{f}(t) = T^*(t)\Sigma(t)\mathbf{f}(t), \qquad \mathbf{f}(t) = \begin{pmatrix} f_+^0(t) \\ \frac{2}{\sqrt{3}} h_+^0(t) \end{pmatrix}. \tag{4.2}$$

The solution of this problem is still accessible with MO techniques when the Omnès function is replaced by an Omnès matrix [60, 61], which in general cannot be given in closed form but has to be determined numerically for a given T-matrix.

According to Fig. 3 the solution of the full RS system requires an iteration between s- and t-channel. However, it was shown in [50] that by far the dominant recoupling between the subsystems proceeds by means of the subtraction constants, while the sensitivity of the t-channel solution on the precise input used for the πN partial waves was found to be very small. Therefore, in the end the accuracy that can be reached for the t-channel amplitudes is limited by the remaining uncertainty in the subthreshold parameters as determined from the iterated RS solution, and effects significantly below that threshold can be neglected. For this reason, the iteration can be organized more efficiently in practice by solving the t-channel system once with reference values for the subthreshold parameters, and then including the corrections to this starting-point solution directly into the solution procedure for the s-channel equations. We use the subthreshold parameters from the KH80 solution [25, 26] as our reference point and express the corrections in terms of

$$\Delta X^{\pm}_{mn} = X^{\pm}_{mn} - X^{\pm}_{mn}\big|_{\mathrm{KH80}}, \qquad X \in \{a, b, d\}. \tag{4.3}$$

The results for the imaginary parts of the t-channel partial waves when the subthreshold parameters are fixed at KH80 values are depicted in Fig. 4. We choose the matching point as $t_\mathrm{m} = t_N$. In general, for the evaluation of the s-channel integrals we use the phase shifts from [27]. For the S-wave, we take the $\pi\pi$ phase shift and inelasticity up to $\sqrt{t_0} = 1.3\,\mathrm{GeV}$ from the Roy-equation analysis of [62] and the $\pi\pi \to \bar{K}K$ partial wave from RS equations [46]. The πN coupling constant is fixed at $g^2/(4\pi) = 13.7$ [48, 49], the KN partial waves are taken from [63], and the hyperon Born terms are evaluated with the couplings from [64]. The main uncertainty is generated by the fact that around 1.3 GeV inelasticities from 4π intermediate states start to become relevant, so that a two-channel description is not strictly applicable any more. For the continuation of the phase shifts above t_0 we consider two extreme cases: first, we guide the phase shifts smoothly to 2π above t_0 (motivated by the asymptotic behavior), and second, we keep the phase shifts constant, with the results represented by the solid and dashed lines in the first panel of Fig. 4, respectively. The variation between these two curves is indeed the largest systematic uncertainty, for instance much larger than the effect of switching off the KN input altogether [65], and will be propagated accordingly in the s-channel error analysis later.

For the P-waves, the largest uncertainty is again generated by 4π inelasticities, which manifest themselves in ρ' and ρ'' resonances that have a substantial branching fraction to 4π. In order to estimate their effect we follow [66] and use a phase shift constructed in such a way as to reproduce the ρ' and ρ'' in the pion vector form factor in an elastic approximation. The results for $\mathrm{Im}\, f^1_\pm(t)$ with (solid lines) and without (dashed lines) these resonances built in are shown in the second row of Fig. 4. The effects are indeed restricted to the energy region above 1 GeV, so that for the error propagation to the s-channel solution the effects are negligible compared to the errors in the subthreshold parameters. The same holds true for the intrinsic uncertainties in the $\pi\pi$ phase shift: using the phase shifts from [40] or [62] produces only tiny differences in the ρ-peak.

The D-waves are dominated by the $f_2(1270)$ resonance, which has a 15% inelasticity to the 4π and $\bar{K}K$ channels. One way to estimate the potential impact of these inelasticities is to replace the $\pi\pi$ phase shift in the MO solution by the phase of the $\pi\pi$ partial wave. The former corresponds to the solid, the latter to the dashed lines in the third row of Fig. 4 (we use phase shift and inelasticity from [40]). The effect is again quite moderate and does not need to be propagated to the s-channel

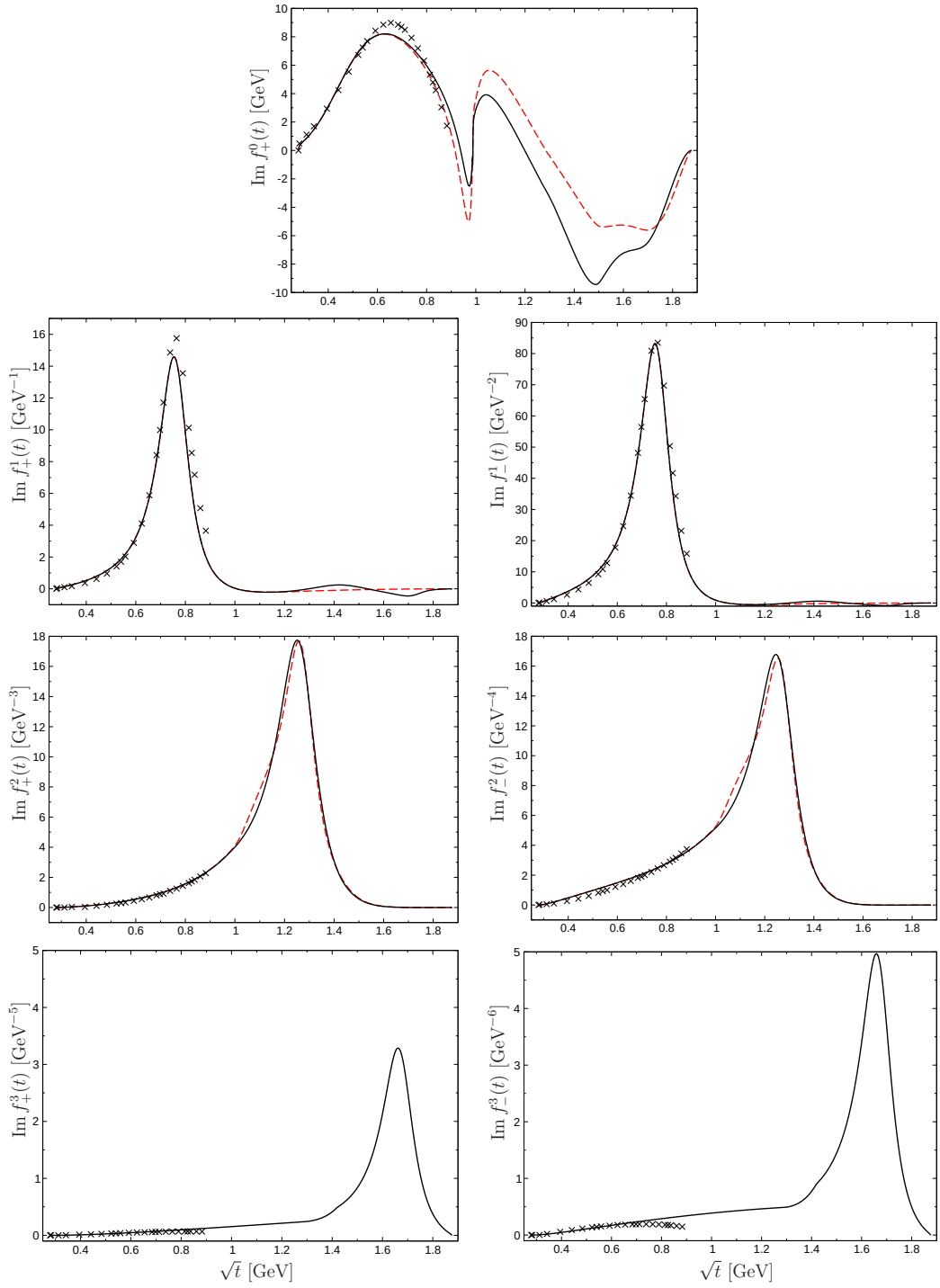

Figure 4: Imaginary parts of the t-channel partial waves with KH80 subthreshold parameters. The black solid (red dashed) line refers to our central solution (the dominant input variation as described in the main text), while the black crosses indicate the results from [26]. Figure taken from [37].

solution. However, we note that the $f_2(1270)$ resonance itself plays an important role in the interplay between the s- and t-channel RS subsystems: without including the $f_2(1270)$ in the t-channel

D-waves, we could not find an acceptable solution of the *s*-channel equations.

In view of this surprising role of the $f_2(1270)$, one may obviously wonder about the impact of yet higher partial waves. The first resonance in the F-waves is the $\rho_3(1690)$, at significantly higher energies than the $f_2(1270)$. Moreover, it is predominantly inelastic with a 70% branching fraction to the 4π channel, so that an elastic treatment becomes difficult to justify. However, to get a rough estimate of the expected size of the F-waves, we constructed an F-wave phase shift by matching the parameterization from [40] to a Breit–Wigner description of the $\rho_3(1690)$, with Breit–Wigner parameters taken from [67] and results shown in the last row of Fig. 4. Indeed, we find that the F-wave contribution is much smaller than the D-wave counterpart, even to the extent that the effect can be safely absorbed into the uncertainty estimate altogether. Given that due to the inelastic nature of the $\rho_3(1690)$ our calculation of the F-waves is less rigorous than that of the lower partial waves, we will indeed quote central results for $J \leq 2$, and only include the F-waves in the error analysis.

Once the t-channel equations are solved, the structure of the s-channel problem resembles the form of $\pi\pi$ Roy equations, and it should be amenable to similar solution techniques. The basic idea can be summarized in such a way that the phase shifts at low energies, from the πN threshold to the maximum allowed matching point at $W_\mathrm{m} = 1.38\,\mathrm{GeV}$, are represented in suitable parameterizations whose free parameters, together with the subtraction constants, are determined by minimizing the difference between the left-hand side (LHS) and right-hand side (RHS) of (3.3),

$$\Delta^2_\mathrm{RS} = \sum_{l,I_s,\pm} \sum_{j=1}^{N} \left(\frac{\mathrm{Re}\, f^{I_s}_{l\pm}(W_j) - F\left[f^{I_s}_{l\pm}\right](W_j)}{\mathrm{Re}\, f^{I_s}_{l\pm}(W_j)} \right)^2 . \tag{4.4}$$

The information required to solve the RS s-channel equations is summarized in the flowchart of Fig. 3. With respect to the s-channel input, in addition to the S- and P-wave inelasticities, we have to include the imaginary part of S- and P-waves above W_m as input, as well as the imaginary parts of the $l > 1$ partial waves above the πN threshold W_+. In the region $W \leq W_\mathrm{a} = 2.5\,\mathrm{GeV}$, we will use the solutions of the Karlsruhe–Helsinki (KH80) [25, 26] and the GWU/SAID [27, 28] PWAs as input. The effect of taking one or the other will be considered as a source of uncertainty. In addition, the significance of higher partial waves decreases as l increases due to the centrifugal barrier. For our central solution we sum up all partial waves up to $l_\mathrm{max} = 4$, while the difference to $l_\mathrm{max} = 5$ is taken as an indication for the truncation error in the partial-wave expansion and will be included in the final uncertainty estimate. Above $W_\mathrm{a} = 2.5\,\mathrm{GeV}$ we consider the Regge model from [68] based on differential cross section and polarization data of backward πN scattering.

With respect to the t-channel contribution, a solution to (3.3) requires information on the imaginary parts of all t-channel partial waves. We use the solutions of the RS t-channel subproblem discussed above as input. The role of the F-waves will be included only as a source of uncertainty, as will be the effect of the different ways to perform the continuation of the S-wave phase shift in the region above $\sqrt{t_0} = 1.3\,\mathrm{GeV}$.

In addition, we found that the solution is stabilized substantially when the S-wave scattering lengths are imposed as constraints on the system instead of trying to predict them from the RS solution. Since the scattering lengths are already known very precisely from pionic atoms [48, 49], a prediction from the RS solution, if it could be extracted in a reliable manner at all, would be

extremely unlikely to be able to compete in accuracy. Therefore we impose on our solutions the scattering length values [49, 69, 37]

$$a_{0+}^{1/2} = (169.8 \pm 2.0) \times 10^{-3} M_\pi^{-1}, \qquad a_{0+}^{3/2} = (-86.3 \pm 1.8) \times 10^{-3} M_\pi^{-1}. \tag{4.5}$$

As the starting point for the minimization, we use KH80 values for the subthreshold parameters, and the GWU/SAID solutions for s-channel phase shifts. In order to investigate to what extent these equations are fulfilled for the SAID s-channel amplitudes, we compare the LHS and RHS of (3.3) before starting the minimization in Fig. 5. This figure shows that the equations are fulfilled in the threshold region (except for the S_{31}-wave), while deviations emerge at higher energies in nearly all partial waves, most notably in the P_{13} and P_{31}.

The minimization of (4.4) provides us with a new set of subthreshold parameters and S- and P-wave phase shifts. The results for the LHS and RHS of the s-channel RS equations after the fit, also shown in Fig. 5, demonstrate good agreement, only for the S_{31}-wave small deviations are still perceptible close to W_m. In addition, Fig. 5 shows that only for the S-waves there is a sizable change between the new solution and the GWU/SAID one. For the P-waves, the agreement between LHS and RHS of the RS s-channel equations is almost entirely due to the change of the subthreshold parameters. This result justifies the approach already introduced above: a solution of the full RS system of equations can be achieved by including the dependence of the t-channel results on the subthreshold parameters explicitly in the minimization of (4.4), but neglecting their weak dependence on the s-channel input, which, in addition, changes little with respect to the SAID values considered in the first place.

5. Results for low-energy phase shifts and subthreshold parameters

The previous results show how to obtain a consistent solution of the t- and s-channel subsystems, by including the dependence of the t-channel partial-wave solutions on the subthreshold parameters explicitly in the s-channel fit. We have performed a full error analysis, where the uncertainty estimates include a number of effects [37]: first, since the RS equations are valid only in a finite energy range below the matching point and only a finite number of partial waves are included explicitly in the solution, we vary the input for the matching condition as well as for the energy region above the matching point and higher partial waves, both regarding different partial-wave analyses and truncations of the partial-wave expansion. Furthermore, we vary the input for the πN coupling constant within $g^2/(4\pi) = 13.7(2)$ [48, 49] and investigate the sensitivity to the parameterization of the low-energy phase shifts used in the solution. Second, we also observed that the RS equations are more sensitive to some subthreshold parameters than others. To account for this effect, we generate a set of solutions corresponding to different starting values of the χ^2-minimization, while imposing sum rules for the higher subthreshold parameters, and took the observed distribution as an additional source of uncertainty. Third, we propagate the errors in the scattering lengths, which crucially enter as constraints in the minimization, to the results for the subthreshold parameters.

The corresponding results for the real parts of the s-channel partial waves are plotted in Fig. 6. The resulting subthreshold parameters are given in Table 1, compared to the KH80 values. The comparison between them reveals fair agreement, all of them lie within 2σ, with the only exception

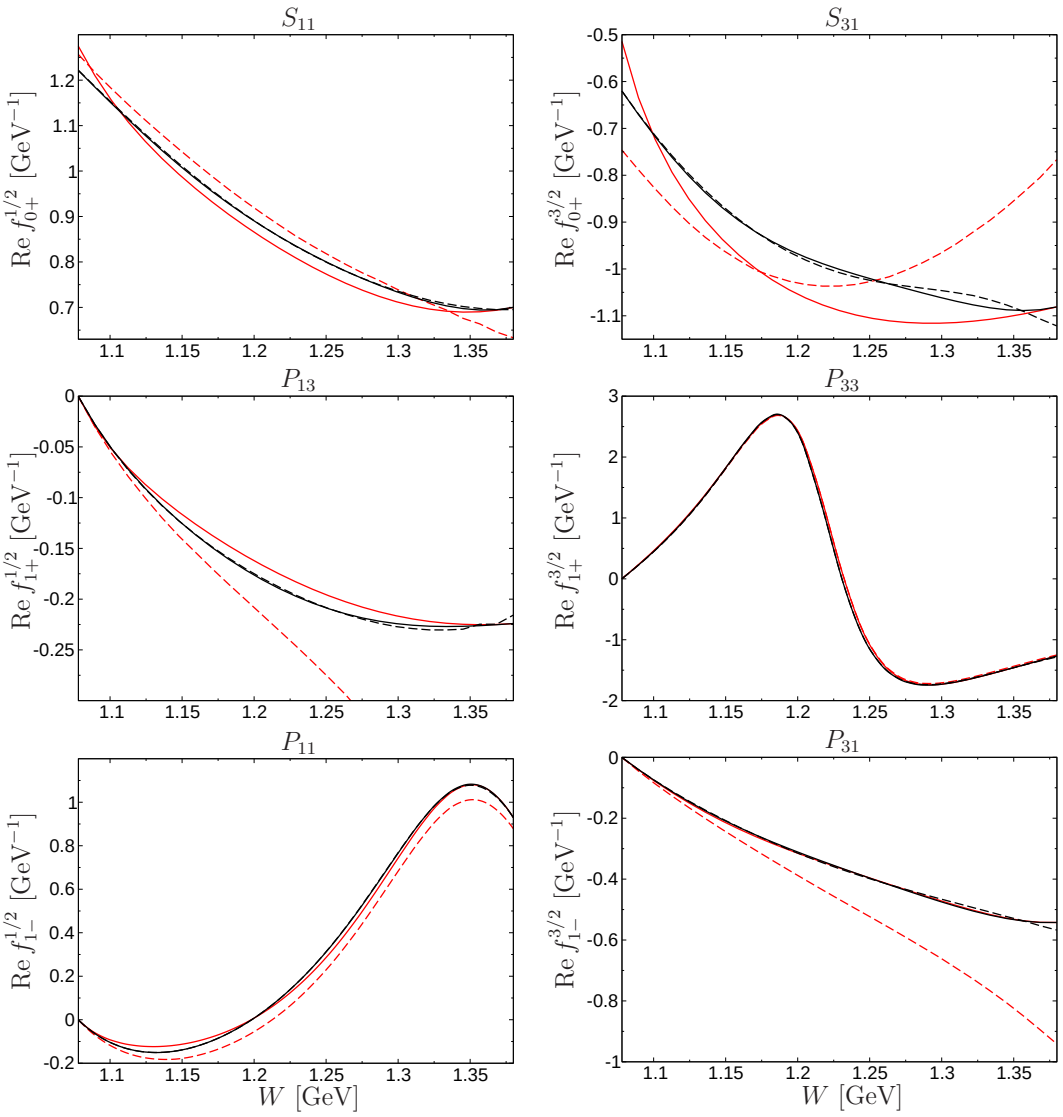

Figure 5: LHS and RHS of the RS equations for Re $f_{l\pm}^{I_s}$. The red solid curves indicate SAID results [27, 28]. Red dashed lines correspond to the RHS of the RS s-channel equations when SAID *s*-channel amplitudes [27, 28] and KH80 [25, 26] subthreshold parameters are considered. Black solid and dashed lines correspond to the LHS and RHS of RS equations after the fit. Figure taken from [37].

of d_{00}^-. We also keep track of the correlations between subthreshold parameters, obtaining a 13×13 covariance matrix that encodes uncertainties and correlations of the 13 subthreshold parameters, which will be relevant for the matching to ChPT.

Once the subthreshold parameters and their covariance matrix are finalized, so can be the uncertainties of the *t*-channel partial waves. They cover both the systematic errors associated with the inelastic input and the $\pi\pi$ phase shifts, as well as the subthreshold-parameter errors. The systematic errors are deduced from the curves depicted in Fig. 4, whose spread is interpreted as a full 1σ band, to be attached around the central solution. For the propagation of the subthreshold-parameter errors we also take into account their correlations, which in particular play a key role for

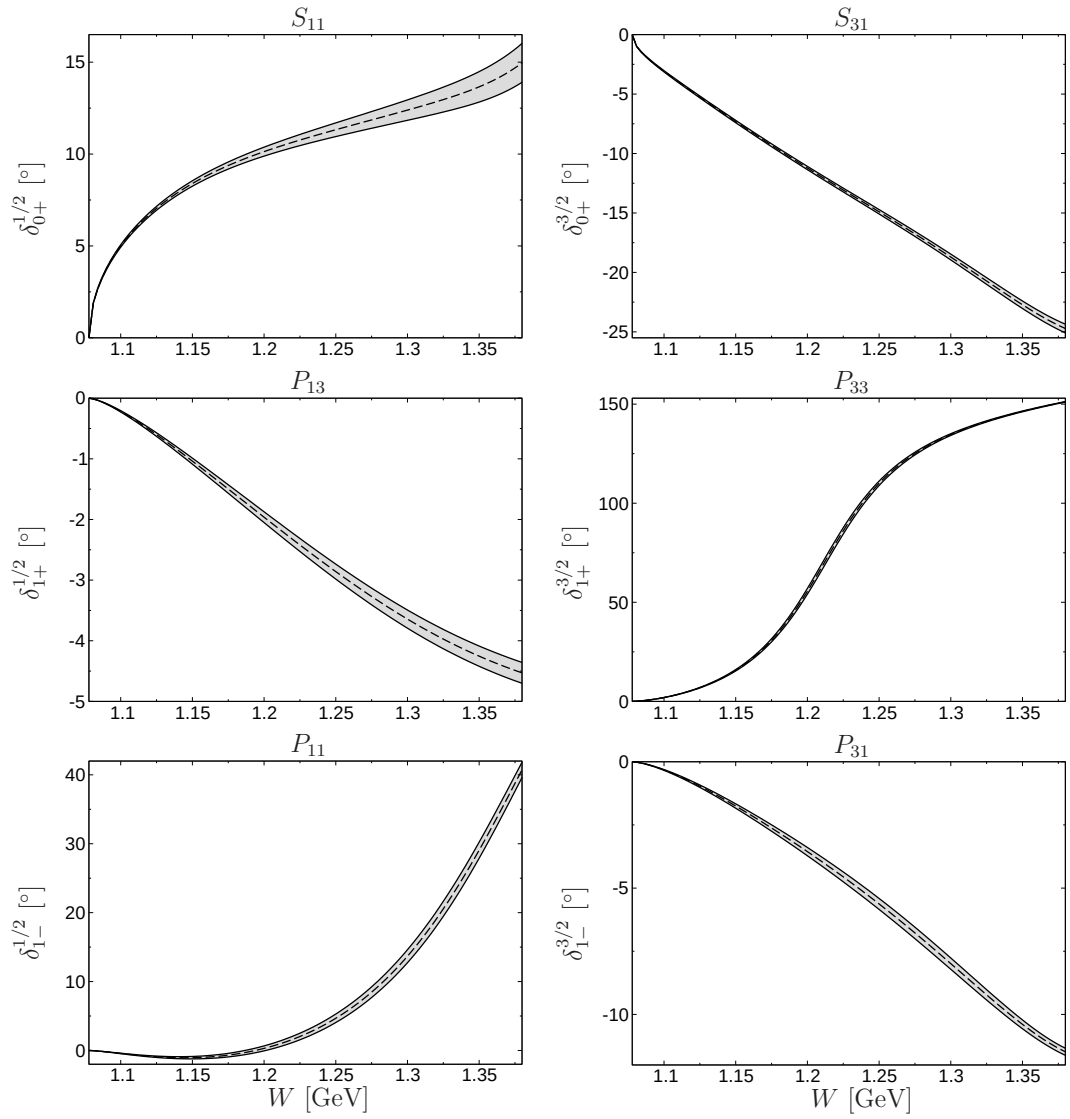

Figure 6: Final errors bands for the πN phase shifts. The dashed lines indicate the central curves. Figure taken from [37].

f_+^1 and f_+^2. We combine both effects by adding them in quadrature, leading to the results for the imaginary parts plotted in Fig. 7.

For completeness we also show the results for the real parts, see Fig. 8. Apart from the *S*-wave all partial waves are strongly dominated by the Born terms close to threshold, where they take a large (but finite) value that would overshadow any structure in the remainder of the amplitude if included in the plot. For this reason, the scale is cut off much earlier, focusing on the part of the partial waves where the respective resonances occur. In general, we find that deviations from the KH80 results are at a similar level as already observed for the imaginary parts, with error analysis performed in the same way as in Fig. 7.

	RS	KH80
$d_{00}^{+}\,[M_\pi^{-1}]$	-1.361 ± 0.032	-1.46 ± 0.10
$d_{10}^{+}\,[M_\pi^{-3}]$	1.156 ± 0.019	1.12 ± 0.02
$d_{01}^{+}\,[M_\pi^{-3}]$	1.155 ± 0.016	1.14 ± 0.02
$d_{20}^{+}\,[M_\pi^{-5}]$	0.196 ± 0.003	0.200 ± 0.005
$d_{11}^{+}\,[M_\pi^{-5}]$	0.185 ± 0.003	0.17 ± 0.01
$d_{02}^{+}\,[M_\pi^{-5}]$	0.0336 ± 0.0006	0.036 ± 0.003
$d_{00}^{-}\,[M_\pi^{-2}]$	1.411 ± 0.015	1.53 ± 0.02
$d_{10}^{-}\,[M_\pi^{-4}]$	-0.159 ± 0.004	-0.167 ± 0.005
$d_{01}^{-}\,[M_\pi^{-4}]$	-0.141 ± 0.005	-0.134 ± 0.005
$b_{00}^{+}\,[M_\pi^{-3}]$	-3.455 ± 0.072	-3.54 ± 0.06
$b_{00}^{-}\,[M_\pi^{-2}]$	10.49 ± 0.11	10.36 ± 0.10
$b_{10}^{-}\,[M_\pi^{-4}]$	1.000 ± 0.029	1.08 ± 0.05
$b_{01}^{-}\,[M_\pi^{-4}]$	0.208 ± 0.020	0.24 ± 0.01

Table 1: Subthreshold parameters from the RS analysis in comparison with the KH80 values [25, 26]. Table taken from [37].

6. Consequences for the πN σ-term

The Cheng–Dashen LET [5, 70] relates the Born-term-subtracted isoscalar amplitude evaluated at the Cheng–Dashen point $(\nu = 0, t = 2M_\pi^2)$ to the scalar form factor of the nucleon, evaluated at momentum transfer $t = (p' - p)^2 = 2M_\pi^2$,

$$\bar{D}^+(0, 2M_\pi^2) = \sigma(2M_\pi^2) + \Delta_R, \tag{6.1}$$

where Δ_R represents higher-order corrections in the chiral expansion. These corrections are expected to be very small: the non-analytic terms agree at full one-loop order [71, 72], so that, based on the $SU(2)$ expansion parameter, the remaining effect would scale as $(M_\pi^2/m_N^2)\sigma_{\pi N} \sim 1\,\text{MeV}$. Here, we use the estimate [71]

$$|\Delta_R| \lesssim 2\,\text{MeV}, \tag{6.2}$$

derived from resonance saturation for the $\mathcal{O}(p^4)$ LECs.

In practice, the relation (6.1) is often rewritten as

$$\sigma_{\pi N} = \sigma(0) = \Sigma_d + \Delta_D - \Delta_\sigma - \Delta_R, \tag{6.3}$$

with correction terms

$$\Delta_\sigma = \sigma(2M_\pi^2) - \sigma_{\pi N}, \qquad \Delta_D = \bar{D}^+(0, 2M_\pi^2) - \Sigma_d, \qquad \Sigma_d = F_\pi^2\big(d_{00}^+ + 2M_\pi^2 d_{01}^+\big). \tag{6.4}$$

	d_{00}^+	d_{10}^+	d_{01}^+	d_{20}^+	d_{11}^+	d_{02}^+	d_{00}^-	d_{10}^-	d_{01}^-	b_{00}^+	b_{00}^-	b_{10}^-	b_{01}^-
d_{00}^+	1	−0.77	−0.51	−0.43	−0.39	−0.30	−0.34	0.43	0.46	0.37	−0.08	−0.39	0.14
d_{10}^+		1	0.85	0.48	0.53	0.58	0.16	−0.40	−0.64	−0.48	0.06	0.56	−0.21
d_{01}^+			1	0.59	0.68	0.90	0.08	−0.55	−0.71	−0.67	0.04	0.58	−0.24
d_{20}^+				1	0.97	0.64	0.14	−0.35	−0.79	−0.63	0.01	0.72	−0.29
d_{11}^+					1	0.67	−0.04	−0.26	−0.79	−0.60	0.01	0.78	−0.28
d_{02}^+						1	0.13	−0.73	−0.75	−0.83	0.06	0.47	−0.22
d_{00}^-							1	−0.50	0.01	−0.23	0.04	−0.11	−0.04
d_{10}^-								1	0.61	0.86	−0.15	−0.05	0.21
d_{01}^-									1	0.86	−0.09	−0.55	0.41
b_{00}^+										1	−0.10	−0.42	0.20
b_{00}^-											1	−0.20	0.34
b_{10}^-												1	0.18
b_{01}^-													1

Table 2: Correlation coefficients for the subthreshold parameters from the RS analysis [37].

Δ_σ measures the curvature in the scalar form factor, while Δ_D parameterizes contributions to the πN amplitude beyond the first two terms in the subthreshold expansion. As shown in [73], although these corrections are large individually due to strong rescattering in the isospin-0 $\pi\pi$ S-wave, they cancel to a large extent in the difference. For the numerical analysis we will use [74, 65]

$$\Delta_D - \Delta_\sigma = (-1.8 \pm 0.2)\,\text{MeV}. \tag{6.5}$$

The crucial remaining challenge thus consists of determining the subthreshold parameters to sufficient accuracy. Based on (6.1) the RS results for the subthreshold parameters translate immediately to a corresponding value of $\sigma_{\pi N}$. To illustrate the dependence of the σ-term on the scattering lengths used as input to the solution, we expand Σ_d linearly around the central values and find

$$\Sigma_d = (57.9 \pm 0.9)\,\text{MeV} + \sum_{I_s} c_{I_s} \Delta a_{0+}^{I_s}, \qquad c_{1/2} = 0.24\,\text{MeV}, \qquad c_{3/2} = 0.89\,\text{MeV}, \tag{6.6}$$

where $\Delta a_{0+}^{I_s}$ gives the deviation from the scattering lenghts extracted from hadronic atoms in units of $10^{-3} M_\pi^{-1}$. Already this linearized version produces $\Sigma_d = (46 \pm 4)\,\text{MeV}$ if the KH80 scattering lengths are used, and the agreement with the original KH80 value $\Sigma_d = (50 \pm 7)\,\text{MeV}$ improves further in a full solution. In contrast, our central solution corresponds to

$$\Sigma_d = (57.9 \pm 1.9)\,\text{MeV}, \tag{6.7}$$

and thus to a significant increase compared to the early estimates.

Including also isospin-breaking corrections [75, 76, 77], the final result [78]

$$\sigma_{\pi N} = (59.1 \pm 3.5)\,\text{MeV}, \tag{6.8}$$

does amount to a significant increase compared to the "canonical value" of $\sigma_{\pi N} \sim 45\,\text{MeV}$, although already 4.2 MeV are due to new corrections to the LET (and thereof 3.0 MeV from isospin

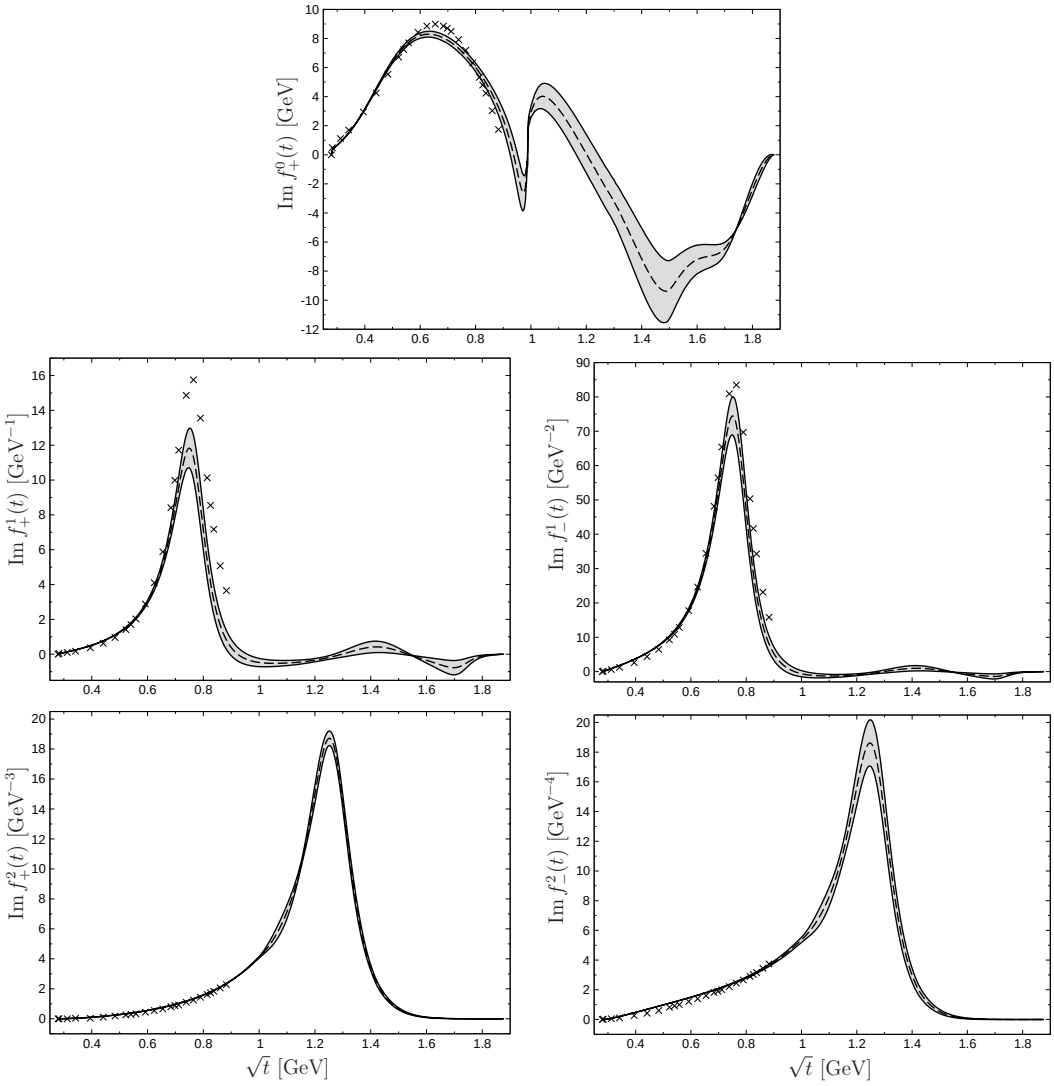

Figure 7: Final results for the imaginary parts of the t-channel partial waves, with error bands including both uncertainties in the subthreshold parameters and the MO input. The black crosses refer to the results from [26]. Figure taken from [37].

breaking). The remaining increase of nearly 10 MeV is dictated by experiment: the new scattering lengths from pionic atoms determine the position of the σ-term on the curve approximately described by (6.6).

As discussed in Sect. 2, the σ-term has also been extracted from πN phase shifts using ChPT at one loop [79, 80, 32], partly finding central values that are compatible with (6.8). All the (dispersive) relations that constitute the Cheng–Dashen LET used in the extraction from the RS solution are fulfilled by the chiral representation, too, albeit only in a perturbative way. In particular, one implicitly needs to extrapolate from the physical s-channel to the subthreshold region. Based on the analysis performed up to here, we point out that the chiral one-loop representation is likely problematic for a precision determination of the σ-term. It is well-known that it does not provide sufficient curvature to the scalar form factor of the nucleon [73]; similarly, the quantity Δ_D

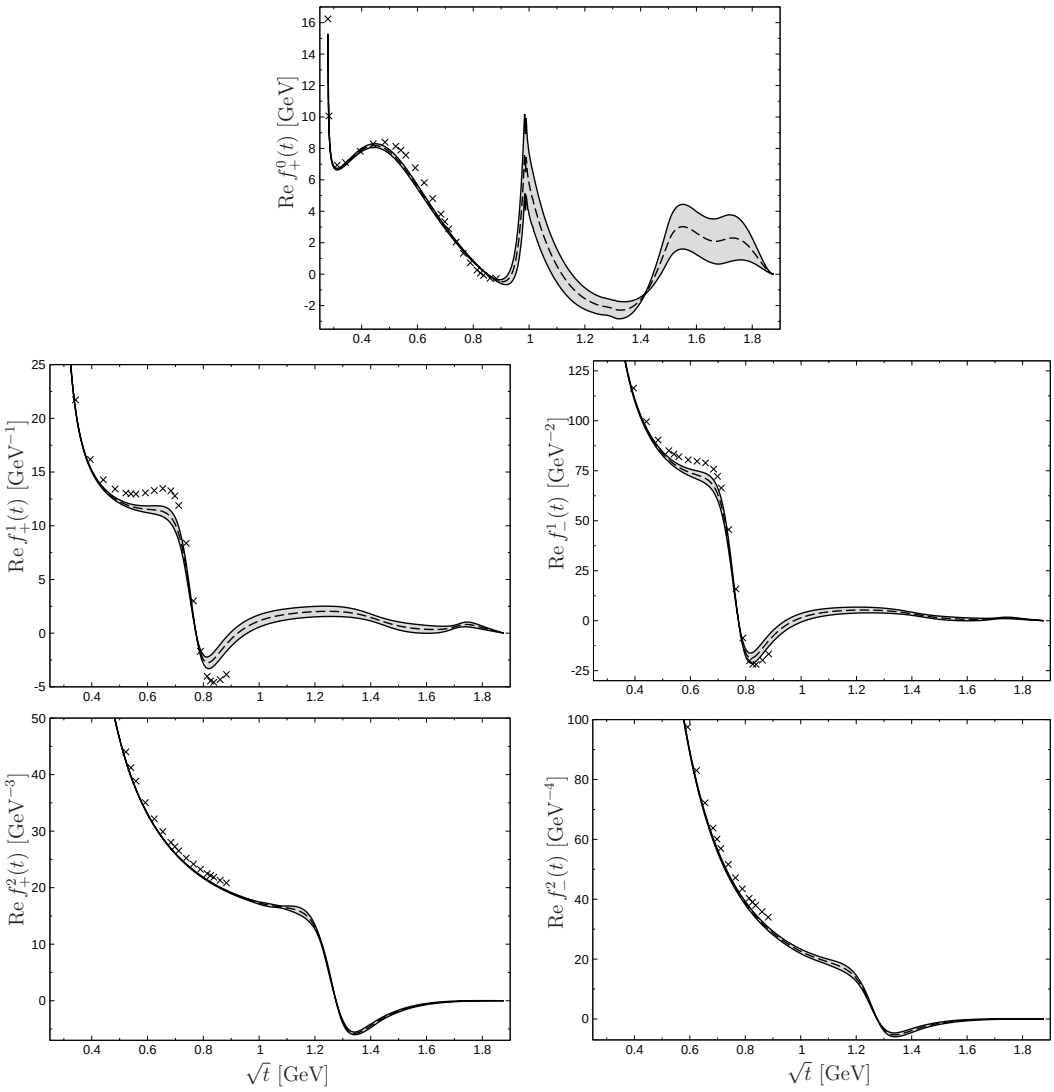

Figure 8: Final results for the real parts of the t-channel partial waves, with error bands including both uncertainties in the subthreshold parameters and the MO input. The black crosses refer to the results from [26]. Figure taken from [37].

is severely underestimated [31]. Therefore, the one-loop representation of the πN scattering amplitude does not describe the subthreshold region very accurately: the extraction of the σ-term is enabled only by the large cancellation in $\Delta_D - \Delta_\sigma$ as described above. Furthermore, the t-channel D-waves including the $f_2(1270)$ resonance are an essential ingredient to a consistent solution of the RS system—omitting its contribution leads to a significantly larger σ-term. The t-channel D-waves of the chiral one-loop representation, however, are real: imaginary parts will only begin to contribute at two-loop order. Hence, the large modifications induced by the $f_2(1270)$ are part of the uncertainties ignored at one loop. The solution to this problem lies in the use of the RS equations for the momentum dependence of the πN amplitude. The convergence of the chiral series as an expansion in powers of the light quark masses can be studied subsequently, as we will see in Sect. 8.

7. On the strangeness content of the nucleon

The πN σ-term can also be related to the mass shift in the nucleon due to strange quarks, $m_s\langle N|\bar{s}s|N\rangle$. For that, one usually considers the so-called strangeness fraction y, given by

$$\sigma_{\pi N} = \frac{\hat{m}}{2m_N}\frac{\langle N|\bar{u}u+\bar{d}d-2\bar{s}s|N\rangle}{1-y} = \frac{\sigma_0}{1-y}, \qquad y \equiv \frac{2\langle N|\bar{s}s|N\rangle}{\langle N|\bar{u}u+\bar{d}d|N\rangle}. \tag{7.1}$$

The leading $SU(3)$ breaking is generated by the operator $(m_s-\hat{m})(\bar{u}u+\bar{d}d-2\bar{s}s)$ so that σ_0 can be expressed through baryon mass splittings

$$\sigma_0 = \frac{\hat{m}}{m_s-\hat{m}}\,(m_\Xi+m_\Sigma-2m_N) \sim 26\,\text{MeV}. \tag{7.2}$$

The first calculation of the higher-order corrections to this relation led to $\sigma_0 = (35\pm5)\,\text{MeV}$ [81], later updated in a modern version of three-flavor baryon ChPT to $\sigma_0 = (36\pm7)\,\text{MeV}$ [82]. Combining this with our value for $\sigma_{\pi N}$ (6.8) would lead to unrealistically large values of the strangeness fraction, $y = 0.4\pm0.1$. However, more recent calculations using covariant baryon ChPT and/or including the effects from the baryon decuplet [83] give sizably larger values of σ_0, for example the covariant calculation of [84] results in $\sigma_0 = (58\pm8)\,\text{MeV}$. Such values for σ_0 lead to very small or even vanishing strangeness fractions. Clearly, in such a scenario our value for $\sigma_{\pi N}$ is not incompatible with a small strangeness fraction, but one also has to realize that the chiral convergence of σ_0 and thus of $m_s\langle N|\bar{s}s|N\rangle$ is very doubtful. Therefore, at present one cannot draw a firm conclusion on the size of y based on (7.1). For this issue, see also the discussion in H. Leutwyler's contribution to these proceedings [85].

8. Matching to chiral perturbation theory

The matching to ChPT is one of the most fundamental applications of the RS solution, since it offers a unique opportunity for a systematic determination of πN LECs [86]. One would expect the chiral expansion to work best in a kinematic region where no singularities occur, i.e. where the amplitude can be described solely by a polynomial in the Mandelstam variables. This is precisely the situation encountered in the subthreshold region: the amplitude is purely real, and characterized by its expansion coefficients around $(\nu=0,t=0)$. The matching is thus most conveniently performed by equating the chiral expansion for the subthreshold parameters to the RS results given in Table 1. In addition, the error propagation will be based on the correlation coefficients listed in Table 2.

As we have discussed already in Sect. 2, the πN amplitude at N^{3}LO, $\mathcal{O}(p^4)$, involves four NLO LECs, c_i, four (combinations of) N^{2}LO LECs, $\bar{d}_i$, and five N^{3}LO LECs, $\bar{e}_i$, see [87]. These 13 LECs correspond to the 13 subthreshold parameters that receive contributions from LECs in a fourth-order calculation (all higher parameters are given by LETs at this order). Inverting the expressions for the subthreshold parameters, we obtain the LECs summarized in Table 3, with correlation coefficients given in [78]. At $O(p^2)$ only the c_i contribute, and only four subthreshold parameters are sensitive to these LECs. In particular, there is a LET for d^-_{00}

$$d^-_{00}\big|_{\text{NLO}} = \frac{1}{2F_\pi^2} = 1.15M_\pi^{-2}, \tag{8.1}$$

	NLO	N^{2}LO	N^{3}LO	N^{3}LO^{NN}
$c_1\,[\mathrm{GeV}^{-1}]$	-0.74 ± 0.02	-1.07 ± 0.02	-1.11 ± 0.03	-1.10 ± 0.03
$c_2\,[\mathrm{GeV}^{-1}]$	1.81 ± 0.03	3.20 ± 0.03	3.13 ± 0.03	3.57 ± 0.04
$c_3\,[\mathrm{GeV}^{-1}]$	-3.61 ± 0.05	-5.32 ± 0.05	-5.61 ± 0.06	-5.54 ± 0.06
$c_4\,[\mathrm{GeV}^{-1}]$	2.17 ± 0.03	3.56 ± 0.03	4.26 ± 0.04	4.17 ± 0.04
$\bar{d}_1+\bar{d}_2\,[\mathrm{GeV}^{-2}]$	—	1.04 ± 0.06	7.42 ± 0.08	6.18 ± 0.08
$\bar{d}_3\,[\mathrm{GeV}^{-2}]$	—	-0.48 ± 0.02	-10.46 ± 0.10	-8.91 ± 0.09
$\bar{d}_5\,[\mathrm{GeV}^{-2}]$	—	0.14 ± 0.05	0.59 ± 0.05	0.86 ± 0.05
$\bar{d}_{14}-\bar{d}_{15}\,[\mathrm{GeV}^{-2}]$	—	-1.90 ± 0.06	-13.02 ± 0.12	-12.18 ± 0.12
$\bar{e}_{14}\,[\mathrm{GeV}^{-3}]$	—	—	0.89 ± 0.04	1.18 ± 0.04
$\bar{e}_{15}\,[\mathrm{GeV}^{-3}]$	—	—	-0.97 ± 0.06	-2.33 ± 0.06
$\bar{e}_{16}\,[\mathrm{GeV}^{-3}]$	—	—	-2.61 ± 0.03	-0.23 ± 0.03
$\bar{e}_{17}\,[\mathrm{GeV}^{-3}]$	—	—	0.01 ± 0.06	-0.18 ± 0.06
$\bar{e}_{18}\,[\mathrm{GeV}^{-3}]$	—	—	-4.20 ± 0.05	-3.24 ± 0.05

Table 3: Results for the πN LECs at different orders in the chiral expansion [86, 37]. In most cases, standard and *NN* counting coincide up to N^{2}LO, except for NLO in c_4, which in the *NN* scheme becomes $(2.44\pm0.03)\,\mathrm{GeV}^{-1}$.

in fair agreement with $d_{00}^- = (1.41\pm0.01)M_\pi^{-2}$ from Table 1.

At N^{2}LO four $\bar{d}_i$ appear, and eight subthreshold parameters receive contributions from LECs. In addition, there are five LETs

$$\begin{aligned} d_{20}^+\big|_{\mathrm{N^2LO}} &= 0.22M_\pi^{-5}, & d_{11}^+\big|_{\mathrm{N^2LO}} &= 0.07M_\pi^{-5}, & d_{02}^+\big|_{\mathrm{N^2LO}} &= 0.034M_\pi^{-5}, \\ b_{10}^-\big|_{\mathrm{N^2LO}} &= 0.92M_\pi^{-4}, & b_{01}^-\big|_{\mathrm{N^2LO}} &= 0.19M_\pi^{-4}, \end{aligned} \tag{8.2}$$

to be compared with the corresponding numbers in Table 1. For all but d_{11}^+ these predictions are quite close to the full result. Comparing the different extractions up to N^{3}LO, the convergence pattern for the c_i looks reasonably stable. In contrast, while the N^{2}LO $\bar{d}_i$ are of natural size, their values increase by nearly an order of magnitude when going to N^{3}LO (except for $\bar{d}_5$). The origin of this behavior can be identified from the analytic expressions, d_{00}^-, d_{10}^-, d_{01}^-, and b_{00}^+ receive loop corrections involving terms that scale with $g_A^2(c_3-c_4)\sim-16\,\mathrm{GeV}^{-1}$, which are balanced by the large LECs in order to keep the subthreshold parameters at their physical values. The enhancement of the c_i, in turn, can be understood from resonance saturation, since, absent low-lying resonant states, they would be expected to scale as $c_i\sim g_A/\Lambda_\mathrm{b}=\mathcal{O}(1\,\mathrm{GeV}^{-1})$ [88]. While t-channel resonances are required as well to reproduce the physical values of the c_i, the most prominent enhancement for c_{2-4} is generated by the $\Delta(1232)$ [89, 21, 16]. Given such large loop corrections the errors for the LECs at a given chiral order are negligible compared to the uncertainties to be attached to the chiral expansion itself.

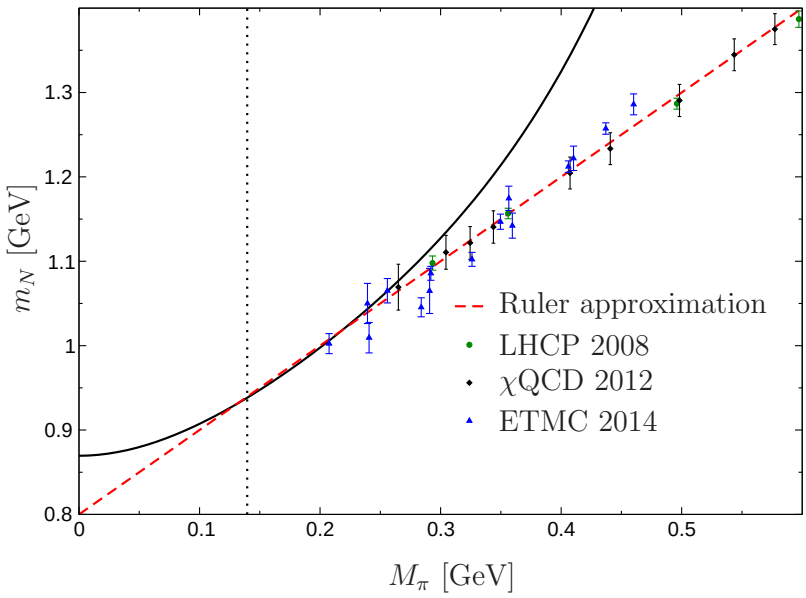

Figure 9: Convergence of the chiral expansion for the nucleon mass as a function of M_π in comparison to lattice: LHCP [92], χQCD [93], and ETMC [94]. Calculations close to or even at the physical point do reproduce the physical mass of the nucleon: 953(41) MeV [95], 936(25)(22) MeV [96], 933(8)(18) MeV [97, 98]. Figure taken from [37].

9. Chiral extrapolation of the nucleon mass

At fourth order in the chiral expansion the nucleon mass can be expressed as [90, 91, 72]

$$m_N = m - 4c_1M_\pi^2 - \frac{3g_A^2M_\pi^3}{32\pi F_\pi^2} - \frac{3}{32\pi^2F_\pi^2 m}\Big(g_A^2 + m(-8c_1+c_2+4c_3)\Big)M_\pi^4\log\frac{M_\pi}{m} + \left\{e_1 - \frac{3}{128\pi^2F_\pi^2 m}\big(2g_A^2 - c_2 m\big)\right\}M_\pi^4 + \mathcal{O}\big(M_\pi^5\big). \tag{9.1}$$

Here, m denotes the nucleon mass in the chiral limit, and M_π, F_π, and g_A are the physical quantities; the renormalization of F_π and g_A is of higher order in the chiral expansion. $e_1 = e_1(m)$ represents a combination of e_i from [87] (evaluated at renormalization scale $\mu = m$).

The chiral expansion of the σ-term as defined in (1.2) follows from (9.1) by means of the Feynman–Hellmann theorem [3, 4]. Since e_1 cannot be determined from the subthreshold parameters of πN scattering, we fix it by demanding that it reproduces (6.8). With e_1 adjusted in this way, we can then predict the nucleon mass in the chiral limit. Including isospin-breaking corrections omitted in (9.1) for simplicity, we obtain [37]

$$\tilde{m} = 869.5\,\text{MeV}, \tag{9.2}$$

where $\tilde{m}$ coincides with m in the isospin limit; see [37] for details.

The full pion-mass dependence is shown in Fig. 9 compared to lattice results. The striking feature coined the "ruler approximation" [99, 100, 101] is that the straight line $800\,\text{MeV} + M_\pi$ reproduces lattice results over a wide range of pion masses, before around the physical region the curvature demanded by ChPT has to set in. This behavior has been confirmed in many more

lattice calculations, see e.g. [95, 96, 94]. Figure 9 demonstrates that the $\mathcal{O}(p^4)$ prediction fails already at pion masses as low as 300 MeV. As noted earlier [102, 88], the range of convergence of the chiral expansion for the nucleon mass appears to be extremely limited. The fact that to a remarkably good approximation lattice results fall on a straight line implies that including higher chiral orders [103, 104, 105, 106] in a fit to lattice data is not a solution:[2] there have to be huge cancellations amongst the individual terms to produce the observed linear behavior.

We stress that this phenomenon solely concerns the range of convergence in M_π, not the rate of convergence at the physical point. Based on the isospin-limit versions of (9.1) and the equivalent expansion of the σ-term, we find

$$m_N = \underbrace{869.5\,\text{MeV}}_{\mathcal{O}(M_\pi^0)} \underbrace{+86.5\,\text{MeV}}_{\mathcal{O}(M_\pi^2)} \underbrace{-15.4\,\text{MeV}}_{\mathcal{O}(M_\pi^3)} \underbrace{-2.3\,\text{MeV}}_{\mathcal{O}(M_\pi^4)} = 938.3\,\text{MeV} \tag{9.3}$$

and

$$\sigma_{\pi N} = \underbrace{86.5\,\text{MeV}}_{\mathcal{O}(M_\pi^2)} \underbrace{-23.2\,\text{MeV}}_{\mathcal{O}(M_\pi^3)} \underbrace{-4.2\,\text{MeV}}_{\mathcal{O}(M_\pi^4)} = 59.1\,\text{MeV}, \tag{9.4}$$

both of which display a very reasonable convergence pattern.

10. Conclusions

Pion–nucleon Roy–Steiner equations allow one to determine the low-energy πN scattering amplitude with high precision. They are based on a rigorous formalism that obeys all the strictures from analyticity, unitarity, and crossing symmetry. New experimental input on the scattering lengths derived from hadronic atoms provides crucial constraints for this analysis. We have for the first time provided πN phase shift at low energies with well-defined systematic uncertainties; explicit numerical parameterizations of these solutions can now be used in various applications [37]. Similarly, the t-channel $\pi\pi \to \bar{N}N$ partial waves have been discussed including a complete error analysis. A new phenomenological determinaton of the πN σ-term has resulted in the very precise value of $\sigma_{\pi N} = (59.1 \pm 3.5)\,\text{MeV}$ [78]. Important checks compared to the previous dispersive Karlsruhe–Helsinki analysis have been performed, in particular we have tested that reverting to older input quantities leads to consistent results throughout. The chiral low-energy constants accessible in pion–nucleon scattering have been determined by matching at the subthreshold point, where convergence of the chiral expansion is expected to work best [86]; the resulting values should be used consistently in future applications of chiral potentials in nuclear physics.

Acknowledgments

We would like to thank the organizers of Chiral Dynamics 2015 in Pisa for a wonderful workshop, and for the invitations to talk about our work on pion–nucleon scattering. Financial support by the Helmholtz Virtual Institute NAVI (VH-VI-417), the DFG (SFB/TR 16, "Subnuclear Structure of Matter"), and the DOE (Grant No. DE-FG02-00ER41132) is gratefully acknowledged.

[2] In principle, we could have included the fifth-order term since it does not involve new unknown LECs. However, this would not be fully consistent because then c_1 and e_1 would need to be extracted from a fifth-order calculation of πN scattering and the σ-term as well.

References

[1] S. Weinberg, Phys. Rev. Lett. **17** (1966) 616.

[2] Y. Tomozawa, Nuovo Cim. A **46** (1966) 707.

[3] H. Hellmann, *Einführung in die Quantenchemie*, Franz Deuticke, Leipzig, 1937.

[4] R. P. Feynman, Phys. Rev. **56** (1939) 340.

[5] T. P. Cheng and R. F. Dashen, Phys. Rev. Lett. **26** (1971) 594.

[6] A. Bottino, F. Donato, N. Fornengo and S. Scopel, Astropart. Phys. **13** (2000) 215 [hep-ph/9909228].

[7] J. R. Ellis, K. A. Olive and C. Savage, Phys. Rev. D **77** (2008) 065026 [arXiv:0801.3656 [hep-ph]].

[8] A. Crivellin, M. Hoferichter and M. Procura, Phys. Rev. D **89** (2014) 054021 [arXiv:1312.4951 [hep-ph]].

[9] S. Weinberg, Physica A **96** (1979) 327.

[10] J. Gasser and H. Leutwyler, Annals Phys. **158** (1984) 142.

[11] J. Gasser and H. Leutwyler, Nucl. Phys. B **250** (1985) 465.

[12] J. Gasser, M. E. Sainio and A. Švarc, Nucl. Phys. B **307** (1988) 779.

[13] E. E. Jenkins and A. V. Manohar, Phys. Lett. B **255** (1991) 558.

[14] V. Bernard, N. Kaiser, J. Kambor and U.-G. Meißner, Nucl. Phys. B **388** (1992) 315.

[15] P. J. Ellis and H. B. Tang, Phys. Rev. C **57** (1998) 3356 [arXiv:hep-ph/9709354].

[16] T. Becher and H. Leutwyler, Eur. Phys. J. C **9** (1999) 643 [hep-ph/9901384].

[17] J. Gegelia and G. Japaridze, Phys. Rev. D **60** (1999) 114038 [hep-ph/9908377].

[18] T. Fuchs, J. Gegelia, G. Japaridze and S. Scherer, Phys. Rev. D **68** (2003) 056005 [hep-ph/0302117].

[19] V. Bernard, N. Kaiser and U.-G. Meißner, Nucl. Phys. A **611** (1996) 429 [hep-ph/9607428].

[20] B. Kubis and U.-G. Meißner, Nucl. Phys. A **679** (2001) 698 [hep-ph/0007056].

[21] V. Bernard, N. Kaiser and U.-G. Meißner, Nucl. Phys. A **615** (1997) 483 [hep-ph/9611253].

[22] E. E. Jenkins and A. V. Manohar, Phys. Lett. B **259** (1991) 353.

[23] T. R. Hemmert, B. R. Holstein and J. Kambor, Phys. Lett. B **395** (1997) 89 [hep-ph/9606456].

[24] V. Pascalutsa and D. R. Phillips, Phys. Rev. C **67** (2003) 055202 [nucl-th/0212024].

[25] R. Koch and E. Pietarinen, Nucl. Phys. A **336** (1980) 331.

[26] G. Höhler, *Pion–Nukleon-Streuung: Methoden und Ergebnisse*, in Landolt-Börnstein, **9b2**, ed. H. Schopper, Springer Verlag, Berlin, 1983.

[27] R. A. Arndt, W. J. Briscoe, I. I. Strakovsky and R. L. Workman, Phys. Rev. C **74** (2006) 045205 [nucl-th/0605082].

[28] R. L. Workman, R. A. Arndt, W. J. Briscoe, M. W. Paris and I. I. Strakovsky, Phys. Rev. C **86** (2012) 035202 [arXiv:1204.2277 [hep-ph]].

[29] E. Matsinos, W. S. Woolcock, G. C. Oades, G. Rasche and A. Gashi, Nucl. Phys. A **778** (2006) 95 [hep-ph/0607080].

[30] J. M. Alarcón, J. Martín Camalich, J. A. Oller and L. Alvarez-Ruso, Phys. Rev. C **83** (2011) 055205 [Phys. Rev. C **87** (2013) 5, 059901] [arXiv:1102.1537 [nucl-th]].

[31] J. M. Alarcón, J. Martin Camalich and J. A. Oller, Annals Phys. **336** (2013) 413 [arXiv:1210.4450 [hep-ph]].

[32] Y. H. Chen, D. L. Yao and H. Q. Zheng, Phys. Rev. D **87** (2013) 054019 [arXiv:1212.1893 [hep-ph]].

[33] J. J. Sanz-Cillero, D. L. Yao and H. Q. Zheng, Eur. Phys. J. C **74** (2014) 2763 [arXiv:1312.0664 [hep-ph]].

[34] H. Krebs, A. Gasparyan and E. Epelbaum, Phys. Rev. C **85** (2012) 054006 [arXiv:1203.0067 [nucl-th]].

[35] K. A. Wendt, B. D. Carlsson and A. Ekström, arXiv:1410.0646 [nucl-th].

[36] A. Gasparyan and M. F. M. Lutz, Nucl. Phys. A **848** (2010) 126 [arXiv:1003.3426 [hep-ph]].

[37] M. Hoferichter, J. Ruiz de Elvira, B. Kubis and U.-G. Meißner, arXiv:1510.06039 [hep-ph].

[38] S. M. Roy, Phys. Lett. B **36** (1971) 353.

[39] B. Ananthanarayan, G. Colangelo, J. Gasser and H. Leutwyler, Phys. Rept. **353** (2001) 207 [hep-ph/0005297].

[40] R. García-Martín, R. Kamiński, J. R. Peláez, J. Ruiz de Elvira, and F. J. Ynduráin, Phys. Rev. D **83** (2011) 074004 [arXiv:1102.2183 [hep-ph]].

[41] M. Froissart, Phys. Rev. **123** (1961) 1053.

[42] A. Martin, Phys. Rev. **129** (1963) 1432.

[43] Y. S. Jin and A. Martin, Phys. Rev. **135** (1964) B1375.

[44] H. Lehmann, Nuovo Cim. **10** (1958) 579.

[45] G. E. Hite and F. Steiner, Nuovo Cim. A **18** (1973) 237 [CERN-TH-1590 for appendices D and E].

[46] P. Büttiker, S. Descotes-Genon and B. Moussallam, Eur. Phys. J. C **33** (2004) 409 [hep-ph/0310283].

[47] M. Hoferichter, D. R. Phillips and C. Schat, Eur. Phys. J. C **71** (2011) 1743 [arXiv:1106.4147 [hep-ph]].

[48] V. Baru *et al.*, Phys. Lett. B **694** (2011) 473 [arXiv:1003.4444 [nucl-th]].

[49] V. Baru *et al.*, Nucl. Phys. A **872** (2011) 69 [arXiv:1107.5509 [nucl-th]].

[50] C. Ditsche, M. Hoferichter, B. Kubis and U.-G. Meißner, JHEP **1206** (2012) 043 [arXiv:1203.4758 [hep-ph]].

[51] C. Ditsche, M. Hoferichter, B. Kubis and U.-G. Meißner, PoS **CD 12** (2013) 064 [arXiv:1211.7285 [hep-ph]].

[52] J. Ruiz de Elvira, C. Ditsche, M. Hoferichter, B. Kubis and U.-G. Meißner, EPJ Web Conf. **73** (2014) 05002.

[53] J. Ruiz de Elvira, C. Ditsche, M. Hoferichter, B. Kubis and U.-G. Meißner, Singapore, Singapore: World Scientific (2014) 186.

[54] J. Stahov, PiN Newslett. **15** (1999) 13.

[55] J. Stahov, PiN Newslett. **16** (2002) 116.

[56] G. E. Hite, W. B. Kaufmann and R. J. Jacob, Phys. Rev. C **71** (2005) 065201.

[57] K. M. Watson, Phys. Rev. **95** (1954) 228.

[58] N. I. Muskhelishvili, *Singular Integral Equations*, Wolters-Noordhoff Publishing, Groningen, 1953 [Dover Publications, 2nd edition, 2008].

[59] R. Omnès, Nuovo Cim. **8** (1958) 316.

[60] J. F. Donoghue, J. Gasser and H. Leutwyler, Nucl. Phys. B **343** (1990) 341.

[61] B. Moussallam, Eur. Phys. J. C **14** (2000) 111 [hep-ph/9909292].

[62] I. Caprini, G. Colangelo, and H. Leutwyler, Eur. Phys. J. C **72** (2012) 1860 [arXiv:1111.7160 [hep-ph]].

[63] J. S. Hyslop, R. A. Arndt, L. D. Roper, and R. L. Workman, Phys. Rev. D **46** (1992) 961.

[64] B. Holzenkamp, K. Holinde and J. Speth, Nucl. Phys. A **500** (1989) 485.

[65] M. Hoferichter, C. Ditsche, B. Kubis and U.-G. Meißner, JHEP **1206** (2012) 063 [arXiv:1204.6251 [hep-ph]].

[66] S. P. Schneider, B. Kubis and F. Niecknig, Phys. Rev. D **86** (2012) 054013 [arXiv:1206.3098 [hep-ph]].

[67] K. A. Olive *et al.* [Particle Data Group Collaboration], Chin. Phys. C **38** (2014) 090001.

[68] F. Huang, A. Sibirtsev, J. Haidenbauer, S. Krewald, and U.-G. Meißner, Eur. Phys. J. A **44** (2010) 81 [arXiv:0910.4275 [nucl-th]].

[69] M. Hoferichter, V. Baru, C. Hanhart, B. Kubis, A. Nogga and D. R. Phillips, PoS CD **12** (2013) 093 [arXiv:1211.1145 [nucl-th]].

[70] L. S. Brown, W. J. Pardee and R. D. Peccei, Phys. Rev. D **4** (1971) 2801.

[71] V. Bernard, N. Kaiser and U.-G. Meißner, Phys. Lett. B **389** (1996) 144 [hep-ph/9607245].

[72] T. Becher and H. Leutwyler, JHEP **0106** (2001) 017 [hep-ph/0103263].

[73] J. Gasser, H. Leutwyler and M. E. Sainio, Phys. Lett. B **253** (1991) 260.

[74] M. Hoferichter, C. Ditsche, B. Kubis and U.-G. Meißner, PoS **CD 12** (2013) 069 [arXiv:1211.1485 [nucl-th]].

[75] J. Gasser, M. A. Ivanov, E. Lipartia, M. Mojžiš and A. Rusetsky, Eur. Phys. J. C **26** (2002) 13 [hep-ph/0206068].

[76] M. Hoferichter, B. Kubis and U.-G. Meißner, Phys. Lett. B **678** (2009) 65 [arXiv:0903.3890 [hep-ph]].

[77] M. Hoferichter, B. Kubis and U.-G. Meißner, Nucl. Phys. A **833** (2010) 18 [arXiv:0909.4390 [hep-ph]].

[78] M. Hoferichter, J. Ruiz de Elvira, B. Kubis and U.-G. Meißner, Phys. Rev. Lett. **115** (2015) 092301 [arXiv:1506.04142 [hep-ph]].

[79] N. Fettes and U.-G. Meißner, Nucl. Phys. A **676** (2000) 311 [hep-ph/0002162].

[80] J. M. Alarcón, J. Martin Camalich and J. A. Oller, Phys. Rev. D **85** (2012) 051503 [arXiv:1110.3797 [hep-ph]].

[81] J. Gasser, Annals Phys. **136** (1981) 62.

[82] B. Borasoy and U.-G. Meißner, Annals Phys. **254** (1997) 192 [hep-ph/9607432].

[83] E. E. Jenkins and A. V. Manohar, Phys. Lett. B **281** (1992) 336.

[84] J. M. Alarcón, L. S. Geng, J. Martin Camalich and J. A. Oller, Phys. Lett. B **730** (2014) 342 [arXiv:1209.2870 [hep-ph]].

[85] H. Leutwyler, Talk given at the 8th International Workshop on Chiral Dynamics, Pisa, 2015, and these proceedings.

[86] M. Hoferichter, J. Ruiz de Elvira, B. Kubis and U.-G. Meißner, arXiv:1507.07552 [nucl-th].

[87] N. Fettes, U.-G. Meißner, M. Mojžiš and S. Steininger, Annals Phys. **283** (2000) 273 [Annals Phys. **288** (2001) 249] [hep-ph/0001308].

[88] V. Bernard, Prog. Part. Nucl. Phys. **60** (2008) 82 [arXiv:0706.0312 [hep-ph]].

[89] V. Bernard, N. Kaiser and U.-G. Meißner, Int. J. Mod. Phys. E **4** (1995) 193 [hep-ph/9501384].

[90] S. Steininger, U.-G. Meißner and N. Fettes, JHEP **9809** (1998) 008 [hep-ph/9808280].

[91] J. Kambor and M. Mojžiš, JHEP **9904** (1999) 031 [hep-ph/9901235].

[92] A. Walker-Loud *et al.*, Phys. Rev. D **79** (2009) 054502 [arXiv:0806.4549 [hep-lat]].

[93] M. Gong *et al.* [XQCD Collaboration], Phys. Rev. D **88** (2013) 014503 [arXiv:1304.1194 [hep-ph]].

[94] C. Alexandrou, V. Drach, K. Jansen, C. Kallidonis and G. Koutsou, Phys. Rev. D **90** (2014) 074501 [arXiv:1406.4310 [hep-lat]].

[95] S. Aoki *et al.* [PACS-CS Collaboration], Phys. Rev. D **79** (2009) 034503 [arXiv:0807.1661 [hep-lat]].

[96] S. Dürr *et al.* [BMW Collaboration], Science **322** (2008) 1224 [arXiv:0906.3599 [hep-lat]].

[97] A. Abdel-Rehim *et al.* [ETM Collaboration], arXiv:1507.04936 [hep-lat].

[98] A. Abdel-Rehim *et al.* [ETM Collaboration], arXiv:1507.05068 [hep-lat].

[99] A. Walker-Loud, PoS **LATTICE 2008** (2008) 005 [arXiv:0810.0663 [hep-lat]].

[100] A. Walker-Loud, PoS **CD 12** (2013) 017 [arXiv:1304.6341 [hep-lat]].

[101] A. Walker-Loud, PoS **LATTICE 2013** (2014) 013 [arXiv:1401.8259 [hep-lat]].

[102] S. R. Beane, Nucl. Phys. B **695** (2004) 192 [hep-lat/0403030].

[103] J. A. McGovern and M. C. Birse, Phys. Lett. B **446** (1999) 300 [hep-ph/9807384].

[104] J. A. McGovern and M. C. Birse, Phys. Rev. D **74** (2006) 097501 [hep-lat/0608002].

[105] M. R. Schindler, D. Djukanovic, J. Gegelia and S. Scherer, Phys. Lett. B **649** (2007) 390 [hep-ph/0612164].

[106] M. R. Schindler, D. Djukanovic, J. Gegelia and S. Scherer, Nucl. Phys. A **803** (2008) 68 [arXiv:0707.4296 [hep-ph]].